NASA TM X-467

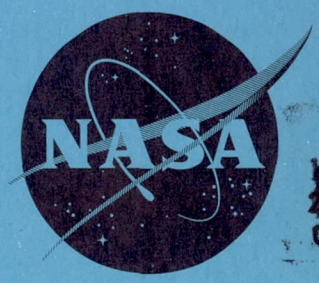

TECHNICAL MEMORANDUM

INVESTIGATION OF THE NORMAL-FORCE, AXIAL-FORCE, AND PITCHING-MOMENT CHARACTERISTICS OF BLUNT LOW-FINENESS-RATIO BODIES OF REVOLUTION AT A MACH NUMBER OF 3.55

By Russell W. McDearmon and Warren A. Lawson

Langley Research Center
Langley Field, Va.

NATIONAL AERONAUTICS AND SPACE ADMINISTRATION

WASHINGTON

April 1961

NATIONAL AERONAUTICS AND SPACE ADMINISTRATION

TECHNICAL MEMORANDUM X-467

INVESTIGATION OF THE NORMAL-FORCE, AXIAL-FORCE, AND PITCHING-MOMENT CHARACTERISTICS OF BLUNT LOW-FINENESS-RATIO BODIES OF REVOLUTION AT A MACH NUMBER OF 3.55*

By Russell W. McDearmon and Warren A. Lawson

SUMMARY

An investigation of the normal-force, axial-force, and pitching-moment characteristics of blunt, low-fineness-ratio bodies of revolution has been made at a Mach number of 3.55. The results indicate that, for cylinders having fineness ratios of 1.00 and 0.50, rounding the corners of the noses caused large decreases in the axial-force coefficients, moderate increases in the slopes of the normal-force curves, and very small changes in the slopes of the pitching-moment curves. Varying the half-angles of cylinder-cone frustums and spherical-faced cone frustums had large effects on the axial-force coefficients and static stability in pitch. For exponential shapes, increasing the exponent from 2 to 10 generally increased the axial-force coefficients, decreased the slopes of the normal-force curves, and decreased the stability in pitch. For a fineness ratio of 1.00 a parabolic body had the least drag, and for a fineness ratio of 0.50 an exponential shape having an exponent of 3 had the least drag. A 26.6° cone and the parabolic body having a fineness ratio of 1.00 had the highest values of normal-force curve slope. All the bodies were statically stable in pitch about a point one-third of the body length rearward from the face, and a spherical-faced cone frustum was the most stable body in pitch. Little variation of axial-force coefficient with angle of attack was obtained for any of the bodies.

Theoretical axial-force and normal-force coefficients were obtained for most of the bodies tested by integrating modified Newtonian pressure distributions on the bodies. Comparisons with the experimental results showed that these predictions were accurate for the parabolic bodies, hemisphere, and hemisphere-cylinder. However, poor agreement between

*Title, Unclassified.

experiment and theory was obtained for the very blunt shapes, such as the flat-faced cylinders and the exponential shapes having exponents of 10, where corner effects were not adequately accounted for in the theory.

INTRODUCTION

Blunt nose shapes have been used extensively for intercontinental ballistic missiles and other reentry vehicles since reference 1 showed that the reentry heating problem could be alleviated by using blunt nose shapes. Consequently, much emphasis has been placed in recent years on obtaining aerodynamic-force and heat-transfer information for various blunt-nose shapes throughout the range of Mach numbers encountered by reentry vehicles in the earth's atmosphere. A general study of the heating and loading for a ballistic missile in the hypersonic phase of its descending trajectory has been made in reference 2. Numerous other theoretical and experimental investigations of the flow over blunt bodies have been carried out, such as the heat-transfer investigations of references 3 and 4, the pressure-distribution investigations of references 5, 6, and 7, and the aerodynamic-force investigations of references 8, 9, and 10.

The purpose of the present investigation was to determine the normal-force, axial-force, and pitching-moment characteristics at a Mach number of 3.55 of a series of blunt low-fineness-ratio bodies. The bodies consisted of cylinders, cylinder-cone frustums, spherical-faced cone frustums, and exponential shapes (including cones). Wind-tunnel measurements of the static longitudinal aerodynamic characteristics at zero yaw of the bodies were made at angles of attack from 0° to 10°. The effects of systematic variations of the following geometric characteristics of the bodies on these static aerodynamic characteristics were determined: for the cylinders, nose corner radius, face contour, and fineness ratio; for the cylinder-cone frustums, half-angle; for the spherical-faced cone frustums, half-angle and fineness ratio; for the exponential shapes, exponent and fineness ratio. The Reynolds number of the tests was 1.12×10^6 per inch.

Theoretical axial-force and normal-force coefficients were obtained for most of the bodies tested by integrating modified Newtonian pressure distributions on the bodies and are compared with the experimental values. For some bodies axial-force and normal-force coefficients obtained by integrating measured pressure distributions (ref. 7) on the bodies are presented.

SYMBOLS

a	a constant in equation of generating curve ($x = ar^n$) for exponential body shapes
F_A	axial force, lb
C_A	axial-force coefficient, $F_A/q_\infty S$
$C_{A_{\alpha=0^\circ}}$	axial-force coefficient for angle of attack of 0°
C_m	pitching-moment coefficient about a point one-third of length of model rearward from face on model center line, $M_x/q_\infty S l$
C_{m_α}	slope of curve of pitching-moment coefficient with angle of attack, per degree
C_N	normal-force coefficient, $F_N/q_\infty S$
C_{N_α}	slope of curve of normal-force coefficient with angle of attack, per degree
C_p	pressure coefficient, $\frac{p - p_\infty}{q_\infty}$
d	diameter of model base, in.
$K = \frac{C_p}{\cos^2\eta}$	
l	length of model, in.
M_x	pitching moment about a point one-third of length of model rearward from face, on model center line
M	Mach number
n	exponent in equation of generating curve ($x = ar^n$) for exponential shapes
F_N	normal force, lb

p	local static pressure, lb/sq in.
p_∞	free-stream static pressure, lb/sq in.
q_∞	free-stream dynamic pressure, lb/sq in.
r	radius, in.
r_1	radius of spherical face of spherical-faced cylinder, cylinder-cone frustum, and cone frustum, in.
r_2	radius of corner of nose of cylinder, cylinder-cone frustum, and cone frustum, in.
S	area of model base, sq in.
x	distance from center of face to surface point on model, measured parallel to model axis, in.
α	angle of attack, deg
η	angle between normal to body surface and free stream, deg

APPARATUS

Wind Tunnel

The tests were conducted in the Mach 3.5 blowdown jet of the Langley Research Center. For this facility, dry air from high-pressure storage tanks is exhausted through a stagnation chamber to a nozzle with a rectangular test section about 5 inches square. The air then passes through a fixed diffuser to the atmosphere. The pressure in the stagnation chamber can be controlled and held constant during a test.

Models

The following types of bodies of revolution were tested: cylinders, cylinder-cone frustums, spherical-faced cone frustums, and exponential shapes. Two fineness ratios, $l/d = 1.00$ and 0.50, were investigated for the cylinders, cone frustums, and exponential shapes, and one fineness ratio, $l/d = 1.00$, was investigated for the cylinder-cone frustums. Drawings of the models are presented in figure 1.

The cylinders consisted of flat-faced cylinders (fig. 1(a)) and spherical-faced cylinders (fig. 1(b)); for the flat-faced cylinders the corner radius was varied from 0 (sharp-cornered) to 0.50d (hemisphere-cylinder for $l/d = 1.00$, hemisphere for $l/d = 0.50$), and for the spherical-faced cylinders the corner radius was varied from 0 to 0.38d.

The cylinder-cone frustums (fig. 1(c)) and the cone frustums (fig. 1(d)) had half-angles of 15° and 30°. The models having $l/d = 1.00$ were formed by adding conical skirts to a cylinder having a spherical face $(r_1/d = 1.00)$ and rounded corner $(r_2/d = 0.20)$; the skirts were located at $l/2$ for the cylinder-cone frustums and were tangent to the corner for the cone frustums. The cone frustums having $l/d = 0.50$ were formed by adding conical skirts tangent to the corner to a cylinder having the same nose shape as the cylinder-cone frustums, but a larger scale.

The exponential shapes (shapes generated by revolving about the x-axis segments of curves having the general equation $x = ar^n$) are presented in figure 1(e). For each fineness ratio, models corresponding to values of n of 1 (cone), 2 (parabolic body), 4, 6, 8, and 10 were tested.

All models were made of stainless steel and were machined to a smooth finish.

TESTS AND ACCURACY

The tests were conducted at a Mach number of 3.55, a stagnation temperature of 55° F, a stagnation pressure of 105 pounds per square inch absolute, and a Reynolds number per inch of 1.12×10^6. For each model the normal forces, axial forces, and pitching moments were measured at angles of attack of 0°, 2°, 4°, 6°, 8°, and 10° by means of an external strain-gage balance. An optical system was used to indicate angle of attack. Base pressures were measured for the models and were used to correct the axial forces measured by the strain-gage balance to the condition of free-stream static pressure acting on the base. Throughout the tests the moisture content in the tunnel was ascertained by dewpoint measurements to be so low that the effects of condensation were negligible.

The measured forces and moments were converted to aerodynamic coefficients, and the estimated probable errors in these coefficients are as follows:

C_N	±0.007
C_A	±0.035
C_m	±0.005

The error in M is ±0.05 and the error in α is ±0.02°.

RESULTS AND DISCUSSION

Figures 2 to 10 present the variations of C_N, C_A, and C_m with angle of attack obtained for all the models tested. The experimental values of C_A have been corrected to the condition of free-stream static pressure acting on the base. The values of C_m are presented about a point one-third of the length of the model behind the face and on the model center line. Also, figures 2 to 10 present theoretical variations of C_N and C_A with angle of attack for most of the models tested. Except for the cones (figs. 9 and 10), these theoretical variations were obtained by integrating modified Newtonian pressure distributions on the models. The charts of reference 9 were used in obtaining the theoretical coefficients, and in the expression for the pressure coefficient $C_p = K \cos^2\eta$, the value of K used was 1.78. For the cones, two predictions of $C_{A_{\alpha=0^\circ}}$ are presented in figures 9 and 10, one based on references 11 and 12 and the other based on unmodified Newtonian theory ($K = 2$). One theoretical variation of C_N with α is presented for each cone, based on references 11 and 12. Figures 2, 4, 6, 7, and 9 include values of C_N and C_A for many of the models having $l/d = 1.00$ which were obtained by integrating measured pressure distributions on identically shaped models; these pressure distributions were presented in reference 7.

Cylinders

Experimental results.- Figures 2 to 5 show the effects on C_N, C_A, and C_m of varying the corner radii of flat-faced and spherical-faced cylinders for $l/d = 1.00$ and 0.50. For both face shapes and both fineness ratios, slightly rounding the corners (increasing r_2/d from 0 to 0.20) caused large decreases in C_A - approximately 30 percent for the flat-faced cylinders and 25 percent for the spherical-faced cylinders. Further increases in the corner radii produced small reductions in C_A. Angle of attack had little effect on C_A for any

of the cylinders. In general, increasing the corner radii increased the slopes of the normal-force curves and had little effect on the slopes of the pitching-moment curves. All the cylinders were stable in pitch.

Comparisons of figure 2 with figure 3 and figure 4 with figure 5 indicate that, for a given nose shape, decreasing the fineness ratio from 1.00 to 0.50 had the following effects: C_A was practically unchanged, C_{N_α} was approximately halved, and the stability in pitch was markedly increased. It might be expected that C_A would be only slightly affected by this change in fineness ratio; however, the marked decrease in C_{N_α} with a decrease in fineness ratio indicates that a larger percentage of the normal force was produced by the cylindrical portion of each body than by the nose.

Comparisons of figure 2 with figure 4 and figure 3 with figure 5 reveal that for both fineness ratios changing the shapes of the faces from flat to spherical gave small reductions in C_A and had little effect on C_{N_α} and C_{m_α}, as would be expected. This result further substantiates the preceding comment that a larger percentage of the normal force was produced by the cylindrical portion than by the face.

Figures 2 and 4 also show that for the cylinders having $l/d = 1.00$ the values of C_A obtained by integrating measured pressure distributions on the models were higher than the values obtained by force measurements. The integrated values of C_N were nearly equal to the values obtained by force measurements. Closer agreement between the integrated and measured values of C_A would probably have been obtained if a greater number of orifices on the noses of the models had been used, particularly near the corners.

Comparisons with theoretical predictions.- Figures 2 to 5 show that theory overpredicted C_A by large amounts for all the cylinders except the hemisphere-cylinder and slightly overpredicted C_A for the hemisphere. Theory underpredicted C_{N_α} for all the cylinders and predicted C_{N_α} almost exactly for the hemisphere; in general, the amount of underprediction increased as the nose bluntness increased. Comparisons of figure 2 with figure 3 and figure 4 with figure 5 show that, for a given nose shape, closer agreement between the experimental and theoretical values of C_{N_α} was obtained for $l/d = 0.50$ than for $l/d = 1.00$.

The large overpredictions of C_A by theory for the sharp-cornered cylinders were expected, since the theory does not account for the decreases in pressure on the rims of the faces which were obtained for these models. (See pressure distributions of ref. 7.) Moreover, reference 7 shows that, for all the cylinders having $l/d = 1.00$ except the hemisphere-cylinder, the pressures on the rims of the faces were lower than those predicted by theory, whereas for the hemisphere-cylinder good agreement between experiment and theory was obtained over the entire nose. Thus theory would be expected to overpredict C_A for all the cylinders except the hemisphere-cylinder and accurately predict C_A for the hemisphere-cylinder and the hemisphere. For the cylinders having slightly rounded corners $(r_2/d = 0.20)$, improved predictions of C_A probably would have been obtained by applying the centrifugal-force correction to the theory.

The accuracies of the theoretical predictions of C_{N_α} are also consistent with the pressure distributions of reference 7. That is, reference 7 shows that on the aft portions of all the cylinders having $l/d = 1.00$, pressures higher than theoretical were obtained on the windward sides, and pressures lower than theoretical were obtained on the leeward sides, for $\alpha = 6^\circ$; this result was most pronounced for the blunt, sharp-cornered cylinders and least pronounced for the hemisphere-cylinder. Good agreement between experiment and theory was obtained over the entire nose of the hemisphere-cylinder. Hence the theoretical values of C_{N_α} would be expected to be much smaller than the measured values for the blunt, sharp-cornered cylinders, slightly less than the measured value for the hemisphere-cylinder, and equal to the measured value for the hemisphere. Also, for a given nose shape, closer agreement between the experimental and theoretical values of C_{N_α} for $l/d = 0.50$ than for $l/d = 1.00$ would be expected, since reference 7 showed that for the models having $l/d = 1.00$ the experimental pressure distributions on the forward portions of the models agreed more closely with theory than the experimental pressure distributions on the aft cylindrical portions.

Cylinder-Cone Frustums and Spherical-Faced Cone Frustums

Experimental results.- Figures 6, 7, and 8 show the effects on C_N, C_A, and C_m of varying the half-angles of cylinder-cone frustums and spherical-faced cone frustums. Increasing the half-angles from 0° to 15° caused large decreases in C_A, had little effect on C_{N_α}, and slightly increased the stability in pitch, whereas increasing the

half-angles from 15° to 30° had little effect on C_A and C_{N_α} and caused large increases in the stability in pitch. Obviously, different effects would have been obtained if the coefficients had been based on a constant area rather than on the areas of the model bases.

Figures 6 and 7 show that, for the cylinder-cone frustums and the longer cone frustums, the values of C_A obtained by integrating measured pressure distributions on the models were slightly higher than the values obtained by force measurements; the values of C_N obtained by integration were almost exactly the same as the values obtained by force measurements. Closer agreement between the integrated and measured values of C_A would probably have been obtained if a greater number of orifices on the noses of the models had been used, particularly near the corners.

Comparisons with theoretical predictions.- Figures 6, 7, and 8 show that, in general, theory predicted C_A and C_N very accurately for the cylinder-cone frustum and the cone frustums having half-angles of 30°. However, the high degree of accuracy of the prediction of C_A for the cylinder-cone frustums may be fortuitous, since reference 7 showed that the flow was separated in the vicinity of the juncture of the cylinder and the cone frustum, and the pressures on the cone frustum near the juncture were much lower than those predicted by modified Newtonian theory.

Exponential Shapes

Experimental results.- Figures 9 and 10 show the effects on C_N, C_A, and C_m of varying n and a for shapes generated by curves defined by the equation $x = ar^n$, for $l/d = 1.00$ and 0.50. Excluding the cones ($n = 1$), increasing the bluntness of the models (that is, increasing n from 2 to 10) generally increased C_A and decreased both C_{N_α} and the static stability in pitch. For each fineness ratio, the cone was the most stable exponential shape in pitch. Larger changes in C_{m_α} were obtained by increasing n from 1 to 2 and 2 to 4 than by increasing n from 4 to 6; nearly identical pitching-moment curves were obtained for $n = 6$, 8, and 10. These effects of n on C_m would be anticipated from geometrical considerations of the bodies. That is, increasing n from 1 to 2 and 2 to 4 causes greater reductions in the amount of inclined surface behind the pitch center (the most effective part of the body in producing pitching moment) than increasing n from 4 to 6, and progressively smaller reductions in inclined surface

area behind the pitch center are obtained by increasing n from 6 to 8 and 8 to 10. Also, the effects of n on C_m for bodies having $l/d = 1.00$ are consistent with the pressure distributions of reference 7. That is, reference 7 shows that, on the windward sides of the aft portions of the bodies, increasing α from 0° to 6° caused larger increases in pressure for the cone and the parabolic body (n = 2) than for the bodies having n = 4, 6, 8, and 10. Increasing the angle of attack from 0° to 10° had little effect on C_A for any of the exponential shapes.

Figure 9 shows that for the exponential shapes having $l/d = 1.00$ and n = 1, 2, and 4, the values of C_A and C_N obtained by integrating measured pressure distributions on the models were nearly equal to the values obtained by force measurements.

Comparisons with theoretical predictions.- Comparisons of the measured and theoretical results presented in figures 9 and 10 indicate the following: For each fineness ratio, modified Newtonian theory predicted C_A very accurately for the parabolic body and overpredicted C_A by progressively larger amounts as the bluntness was increased (n increased from 2 to 4 and 4 to 10). For both cones, unmodified Newtonian theory predicted $C_{A_{\alpha=0^\circ}}$ very accurately, whereas the theoretical values of $C_{A_{\alpha=0^\circ}}$ based on references 11 and 12 were slightly higher than the measured values. The measured and modified Newtonian theoretical C_N curves agreed very closely for the bodies having n = 2 and 4, but for the very blunt shapes (n = 10) the theoretical values of C_{N_α} were less than the measured values. The theory based on references 11 and 12 predicted C_{N_α} very accurately for the 26.65° cone ($l/d = 1.00$), but overpredicted C_{N_α} for the 45° cone ($l/d = 0.50$); this result would be expected, since the 45° cone was nearer the condition of nose-shock detachment than the 26.65° cone.

The relative accuracies of the theoretical predictions of C_A for the bodies having $l/d = 1.00$ are consistent with reference 7, in that reference 7 shows (1) that modified Newtonian theory accurately predicted the pressures on the frontal part of the parabolic body and overpredicted the pressures on the frontal parts of the bodies having n = 4 and 10; and (2) both unmodified Newtonian theory and the theory based on references 11 and 12 predicted the pressures on the 26.65° cone very closely.

Experimental and theoretical zero-lift drag.- In order to show the relative magnitudes of the values of zero-lift drag which were obtained

for the exponential shapes tested, plots of the variation of $C_{A_{\alpha=0^\circ}}$ with n for $l/d = 1.00$ and 0.50 are presented in figure 11. Also, for both fineness ratios figure 11 presents modified Newtonian theoretical variations of $C_{A_{\alpha=0^\circ}}$ with n for bodies having values of n ranging from 1.1 to 10 and unmodified Newtonian theoretical values of $C_{A_{\alpha=0^\circ}}$ for the cones (n = 1). The experimental curves indicate that the parabolic body (n = 2) had the least zero-lift drag for $l/d = 1.00$ and that a body having $n \approx 3$ would have the least zero-lift drag for $l/d = 0.50$. The theoretical least-drag body was less blunt than the experimental least-drag body for each fineness ratio (theoretically, $n \approx 1.3$ for $l/d = 1.00$ and $n \approx 2.1$ for $l/d = 0.50$). Thus, both experimentally and theoretically the least-drag bodies were blunter for $l/d = 0.50$ than for $l/d = 1.00$. This result is consistent with that of reference 13, which showed that the minimum-drag bodies at high supersonic speeds for $l/d = 3.00$ and 5.00 were exponential shapes having $n = 1.33$ and predicted that the degree of bluntness of the minimum-drag body would increase with decreasing fineness ratio.

L 9 9 8

Relative Magnitudes of $C_{A_{\alpha=0^\circ}}$, C_{N_α}, and C_{m_α}

In order to show the relative magnitudes of the values of $C_{A_{\alpha=0^\circ}}$, C_{N_α}, and C_{m_α} obtained for the models tested, these values were compiled and are presented in table I.

As would be expected, the flat-faced, sharp-cornered cylinders had the largest values of $C_{A_{\alpha=0^\circ}}$. The spherical-faced sharp-cornered cylinders were second in order of magnitude of $C_{A_{\alpha=0^\circ}}$. The 45° cone had a relatively high value of $C_{A_{\alpha=0^\circ}}$; that is, the cone had approximately the same $C_{A_{\alpha=0^\circ}}$ as the flat-faced cylinders having slightly rounded corners. The smallest value of $C_{A_{\alpha=0^\circ}}$ was obtained for the parabolic body having $l/d = 1.00$.

The 26.6° cone and the parabolic body having $l/d = 1.00$ had the highest values of C_{N_α} and were followed closely by the other exponential shapes having $l/d = 1.00$ and the hemisphere-cylinder. The lowest C_{N_α} was obtained for the flat-faced sharp-cornered cylinder having $l/d = 0.50$.

The shorter spherical-faced cone frustum having a half-angle of 30° was the most stable model in pitch. Both cones and the longer cone

frustum having a half-angle of 30° were next in degree of pitch stability. All the models were stable in pitch, although only very small negative values of C_{m_α} were obtained for the cylinders and near-cylinders having $l/d = 1.00$.

CONCLUSIONS

The results of an investigation of the normal-force, axial-force, and pitching-moment characteristics of blunt low-fineness-ratio bodies at a Mach number of 3.55 indicate the following conclusions:

1. For cylinders having fineness ratios of 1.00 and 0.50, rounding the corners of the noses caused large decreases in the axial-force coefficients C_A, moderate increases in the slopes of the normal-force curves C_{N_α}, and very small changes in the slopes of the pitching-moment curves C_{m_α}. Changing the contours of the faces from flat to spherical caused small decreases in C_A.

2. For cylinder-cone frustums and spherical-faced cone frustums, increasing the half-angles from 0° to 15° produced large reductions in C_A, small changes in C_{N_α}, and slight increases in the static stability in pitch. Increasing the half-angles from 15° to 30° had small effects on C_A and C_{N_α} and caused large increases in the stability in pitch.

3. For exponential shapes having fineness ratios of 1.00 and 0.50, increasing the exponent n from 2 to 10 generally increased C_A, decreased C_{N_α}, and decreased the stability in pitch. Cones ($n = 1$) were the most stable exponential shapes in pitch.

4. For a fineness ratio of 1.00 a parabolic body had the least drag, and for a fineness ratio of 0.50 an exponential shape having $n \approx 3$ had the least drag. A 26.6° cone and the parabolic body having a fineness ratio of 1.00 had the highest values of C_{N_α}. All the bodies were statically stable in pitch about a point one-third of the body length rearward from the face, and the shorter spherical-faced cone frustum having a half-angle of 30° was the most stable body in pitch. Little variation of axial-force coefficient with angle of attack was obtained for any of the bodies.

5. Theoretical predictions of C_A and C_N obtained by integrating modified Newtonian pressure distributions on the bodies were very

accurate for the parabolic bodies, hemisphere, and hemisphere-cylinder but were poor for the very blunt shapes, such as the flat-faced cylinders and the exponential shapes having $n = 10$, where corner effects were not adequately accounted for in the theory.

Langley Research Center,
National Aeronautics and Space Administration,
Langley Field, Va., December 20, 1960.

REFERENCES

1. Allen, H. Julian, and Eggers, A. J., Jr.: A Study of the Motion and Aerodynamic Heating of Ballistic Missiles Entering the Earth's Atmosphere at High Supersonic Speeds. NACA Rep. 1381, 1958. (Supersedes NACA TN 4047.)

2. Allen, H. Julian: Motion of a Ballistic Missile Angularly Misalined With the Flight Path Upon Entering the Atmosphere and Its Effect Upon Aerodynamic Heating, Aerodynamic Loads, and Miss Distance. NACA TN 4048, 1957. (Supersedes NACA RM A56F15.)

3. Lees, Lester: Laminar Heat Transfer Over Blunt-Nosed Bodies at Hypersonic Flight Speeds. Jet Propulsion, vol. 26, no. 4, Apr. 1956, pp. 259-269.

4. Stine, Howard A., and Wanlass, Kent: Theoretical and Experimental Investigation of Aerodynamic Heating and Isothermal Heat-Transfer Parameters on a Hemispherical Nose With Laminar Boundary Layer at Supersonic Mach Numbers. NACA TN 3344, 1954.

5. Cole, J. D.: Newtonian Flow Theory for Slender Bodies. Jour. Aero. Sci., vol. 24, no. 6, June 1957, pp. 448-455.

6. Oliver, Robert Earl: An Experimental Investigation of Flow About Simple Blunt Bodies at a Nominal Mach Number of 5.8. Jour. Aero. Sci. (Readers' Forum), vol. 23, no. 2, Feb. 1956, pp. 177-179.

7. Lawson, Warren A., McDearmon, R. W., and Rainey, R. W.: Investigation of the Pressure Distributions on Reentry Nose Shapes at a Mach Number of 3.55. NASA TM X-244, 1960.

8. Grimminger, G., Williams, E. P., and Young, G. B. W.: Lift on Inclined Bodies of Revolution in Hypersonic Flow. Jour. Aero. Sci., vol. 17, no. 11, Nov. 1950, pp. 675-690.

9. Rainey, Robert W.: Working Charts for Rapid Prediction of Force and Pressure Coefficients on Arbitrary Bodies of Revolution by Use of Newtonian Concepts. NASA TN D-176, 1959.

10. Penland, Jim A.: Aerodynamic Characteristics of a Circular Cylinder at Mach Number 6.86 and Angles of Attack up to 90°. NACA TN 3861, 1957. (Supersedes NACA RM L54A14.)

11. Staff of the Computing Section, Center of Analysis (Under Direction of Zdeněk Kopal): Tables of Supersonic Flow Around Yawing Cones. Tech. Rep. No. 3 (NOrd Contract No. 9169), M.I.T., 1947.

12. Ames Research Staff: Equations, Tables, and Charts for Compressible Flow. NACA Rep. 1135, 1953. (Supersedes NACA TN 1428.)

13. Eggers, A. J., Jr., Resnikoff, Meyer M., and Dennis, David H.: Bodies of Revolution Having Minimum Drag at High Supersonic Speeds. NACA Rep. 1306, 1957. (Supersedes NACA TN 3666.)

TABLE I. - VALUES OF $C_{A_{\alpha=0^\circ}}$, C_{N_α}, AND C_{m_α} OBTAINED FOR THE MODELS TESTED.

Model	$C_{A_{\alpha=0^\circ}}$	C_{N_α}	C_{m_α}
	1.51	0.015	-0.005
	1.04	0.018	-0.004
	0.84	0.019	-0.004
	0.73	0.022	-0.005
	1.35	0.015	-0.005
	0.98	0.019	-0.005
	0.81	0.021	-0.005
	1.08	0.018	-0.001
	0.74	0.017	-0.002
	0.69	0.018	-0.009
	0.52	0.015	-0.003
	0.59	0.020	-0.013
n=1 	0.41	0.025	-0.014
n=2 	0.29	0.025	-0.009
n=4 	0.44	0.022	-0.006
n=6 	0.57	0.021	-0.004
n=8 	0.64	0.020	-0.004
n=10 	0.70	0.020	-0.004

$\frac{l}{d} = 1.00$

Model	$C_{A_{\alpha=0^\circ}}$	C_{N_α}	C_{m_α}
	1.49	0.006	-0.008
	1.06	0.011	-0.008
	0.87	0.014	-0.009
	0.79	0.014	-0.009
	1.32	0.007	-0.008
	1.01	0.011	-0.008
	0.86	0.014	-0.010
	0.78	0.012	-0.009
	0.82	0.014	-0.016
n=1 	1.03	0.014	-0.014
n=2 	0.67	0.017	-0.011
n=4 	0.66	0.016	-0.009
n=6 	0.73	0.013	-0.007
n=8 	0.78	0.013	-0.007
n=10 	0.86	0.013	-0.007

$\frac{l}{d} = 0.50$

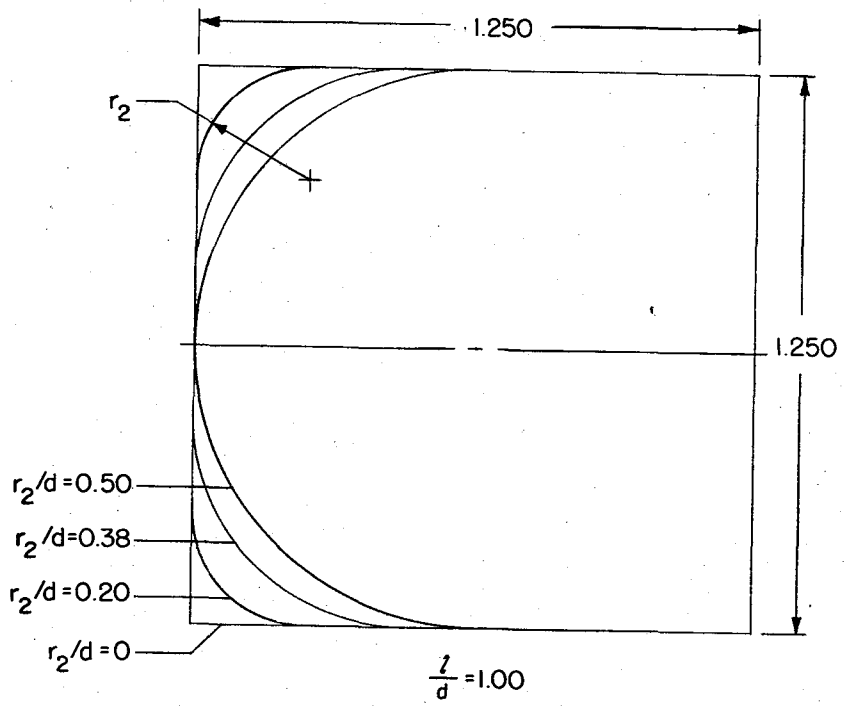

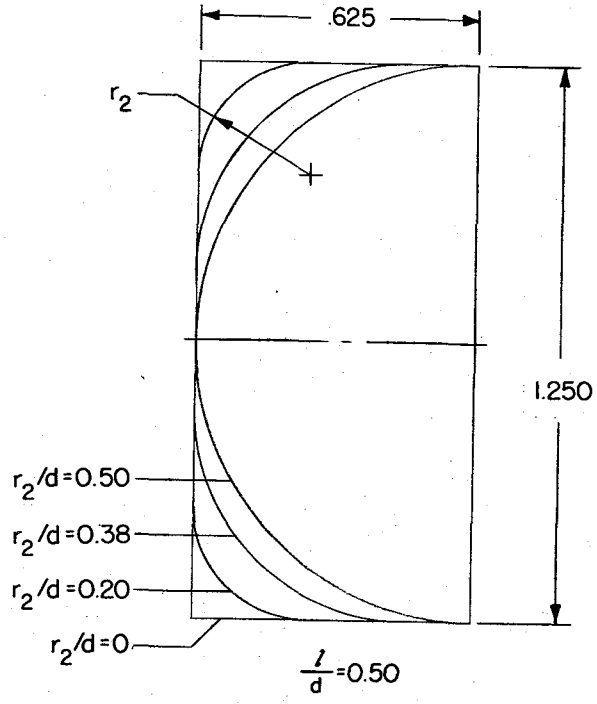

(a) Flat-faced cylinders having various corner radii, hemisphere-cylinder, and hemisphere.

Figure 1.- Drawings of models. All dimensions are in inches.

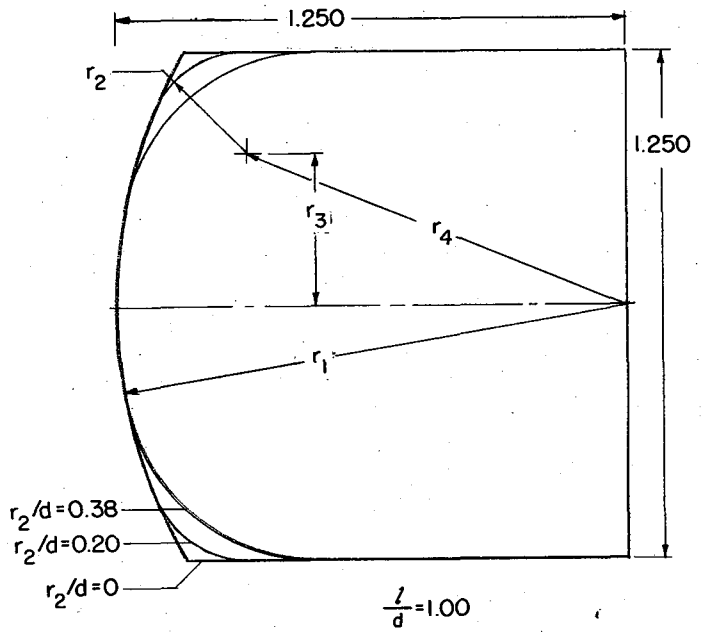

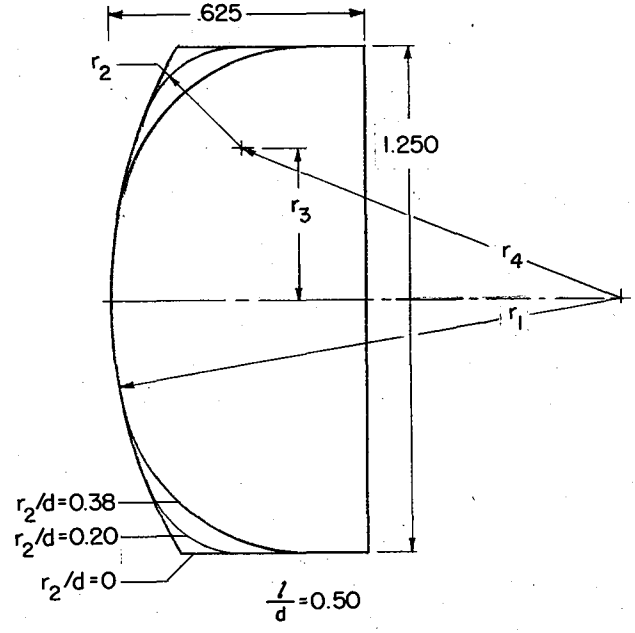

$\frac{r_2}{d}$	r_2	r_3	r_4
0	0		
0.20	.250	.375	1.000
0.38	.469	.156	.781

(b) Spherical-faced cylinders, $r_1/d = 1.00$.

Figure 1.- Continued.

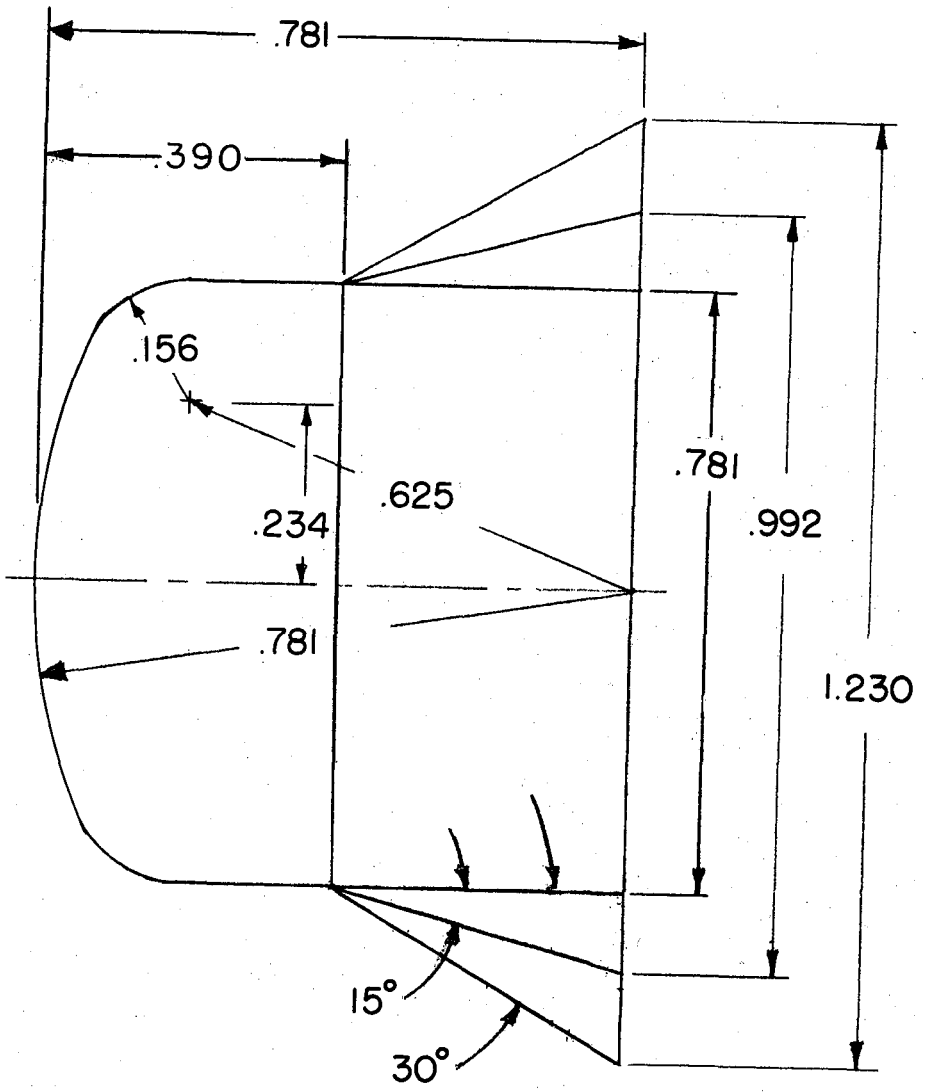

(c) Cylinder-cone frustums. For half-angle of 0°, $r_1/d = 1.00$, $r_2/d = 0.20$, $l/d = 1.00$.

Figure 1.- Continued.

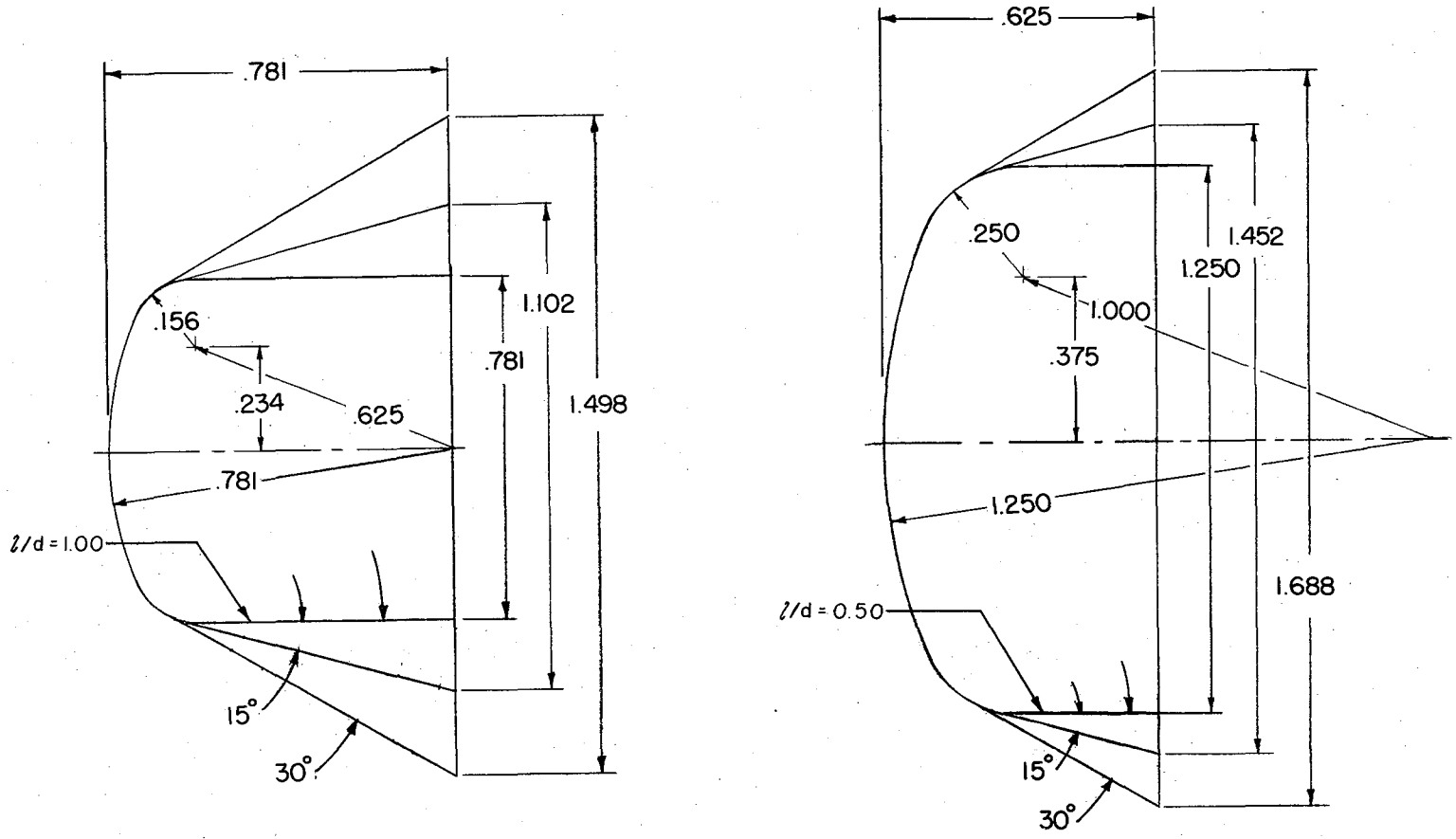

(d) Spherical-faced cone frustrums. For model with half-angle of 0°, $r_1/d = 1.00$, $r_2/d = 0.20$.

Figure 1.- Continued.

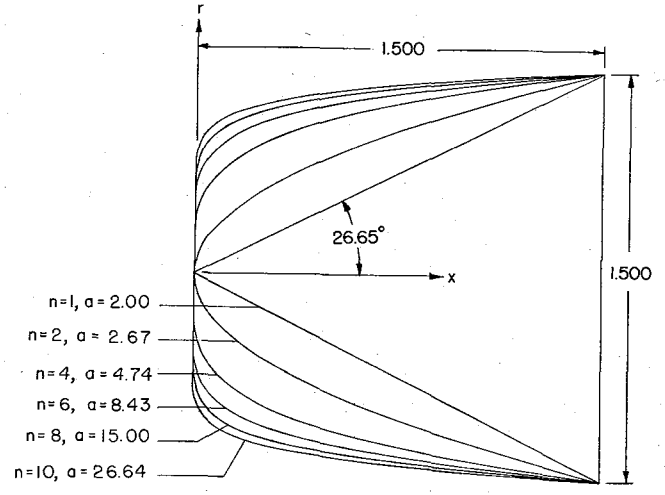

$l/d = 1.00$

Model Ordinates									
n=2, a=2.67		n=4, a=4.74		n=6, a=8.43		n=8, a=15.00		n=10, a=26.64	
x	r	x	r	x	r	x	r	x	r
0	0	0	0	0	0	0	0	0	0
.015	.075	.015	.237	.015	.350	.015	.421	.015	.473
.030	.107	.030	.282	.030	.392	.030	.460	.030	.507
.045	.130	.045	.312	.045	.419	.045	.484	.045	.528
.060	.150	.060	.335	.060	.440	.060	.502	.060	.543
.075	.168	.075	.356	.075	.456	.075	.516	.075	.556
.150	.237	.150	.422	.150	.511	.150	.562	.150	.596
.300	.335	.300	.502	.300	.574	.300	.614	.300	.638
.450	.411	.450	.555	.450	.614	.450	.645	.450	.664
.600	.474	.600	.596	.600	.644	.600	.669	.600	.684
.750	.530	.750	.631	.750	.668	.750	.688	.750	.700
.900	.581	.900	.660	.900	.689	.900	.704	.900	.712
1.050	.627	1.050	.686	1.050	.707	1.050	.717	1.050	.724
1.200	.671	1.200	.709	1.200	.722	1.200	.729	1.200	.734
1.350	.712	1.350	.730	1.350	.736	1.350	.740	1.350	.742
1.500	.750	1.500	.750	1.500	.750	1.500	.750	1.500	.750

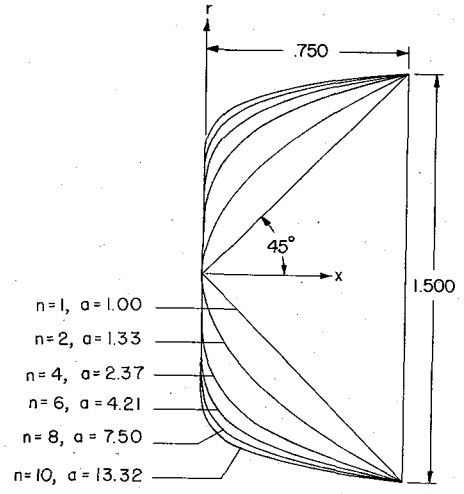

$l/d = 0.50$

Model Ordinates									
n=2, a=1.33		n=4, a=2.37		n=6, a=4.21		n=8, a=7.50		n=10, a=13.32	
x	r	x	r	x	r	x	r	x	r
0	0	0	0	0	0	0	0	0	0
.003	.047	.003	.189	.003	.299	.003	.376	.003	.432
.008	.075	.008	.237	.008	.348	.008	.422	.008	.473
.015	.106	.015	.282	.015	.391	.015	.460	.015	.507
.030	.150	.030	.335	.030	.439	.030	.502	.030	.544
.045	.184	.045	.371	.045	.469	.045	.528	.045	.566
.060	.212	.060	.399	.060	.492	.060	.547	.060	.583
.075	.238	.075	.422	.075	.511	.075	.562	.075	.596
.150	.335	.150	.502	.150	.574	.150	.613	.150	.639
.225	.411	.225	.555	.225	.614	.225	.645	.225	.665
.300	.474	.300	.596	.300	.644	.300	.669	.300	.684
.375	.530	.375	.631	.375	.668	.375	.688	.375	.700
.450	.581	.450	.660	.450	.689	.450	.704	.450	.713
.525	.628	.525	.686	.525	.707	.525	.717	.525	.724
.600	.671	.600	.709	.600	.723	.600	.729	.600	.733
.675	.712	.675	.731	.675	.737	.675	.740	.675	.742
.750	.750	.750	.750	.750	.750	.750	.750	.750	.750

(e) Exponential shapes (shapes generated by revolving about the x-axis segments of curves having the general equation $x = ar^n$).

Figure 1.- Concluded.

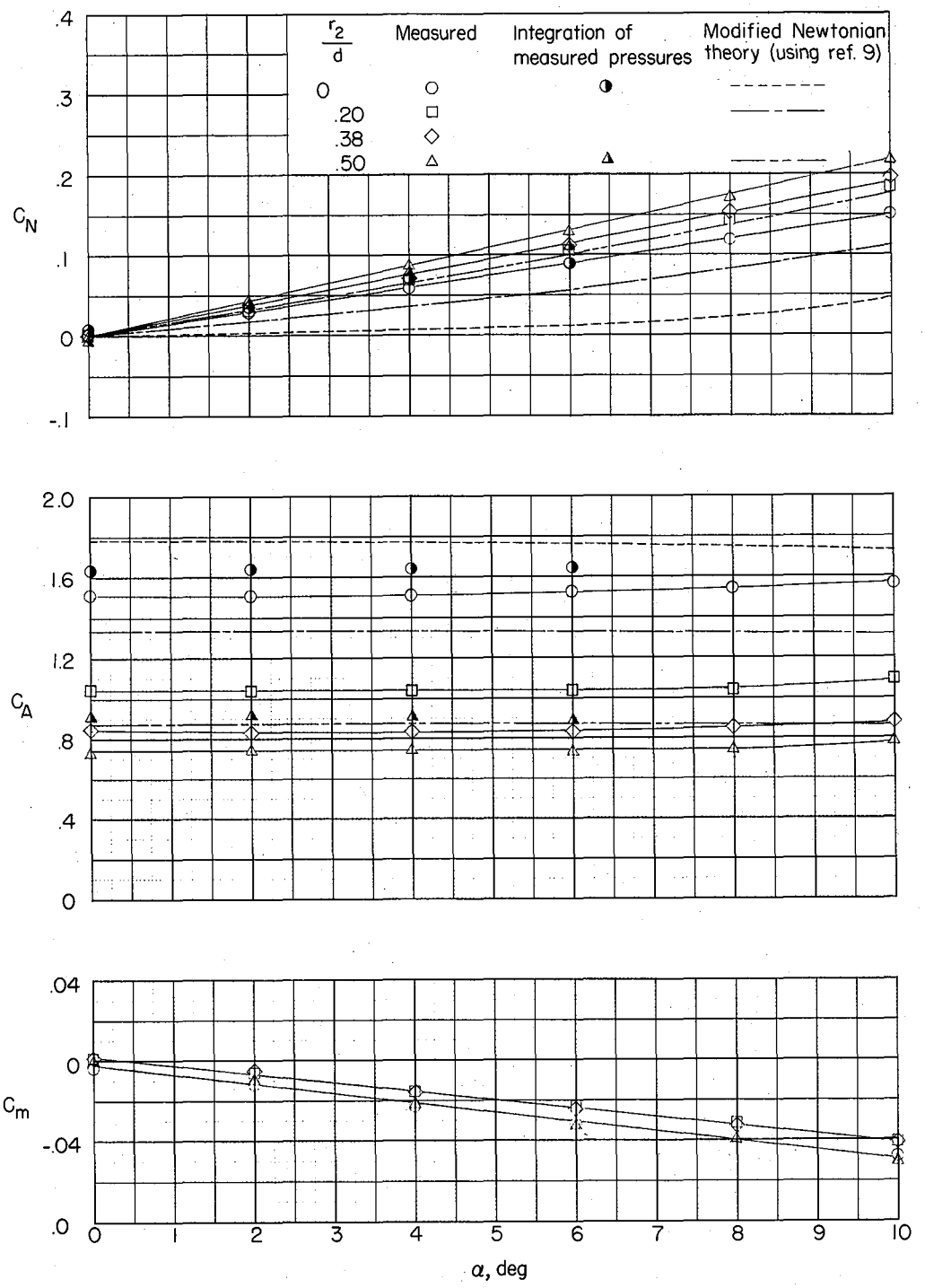

Figure 2.- Effects on C_N, C_A, and C_m of varying the corner radius of flat-faced cylinder having $l/d = 1.00$.

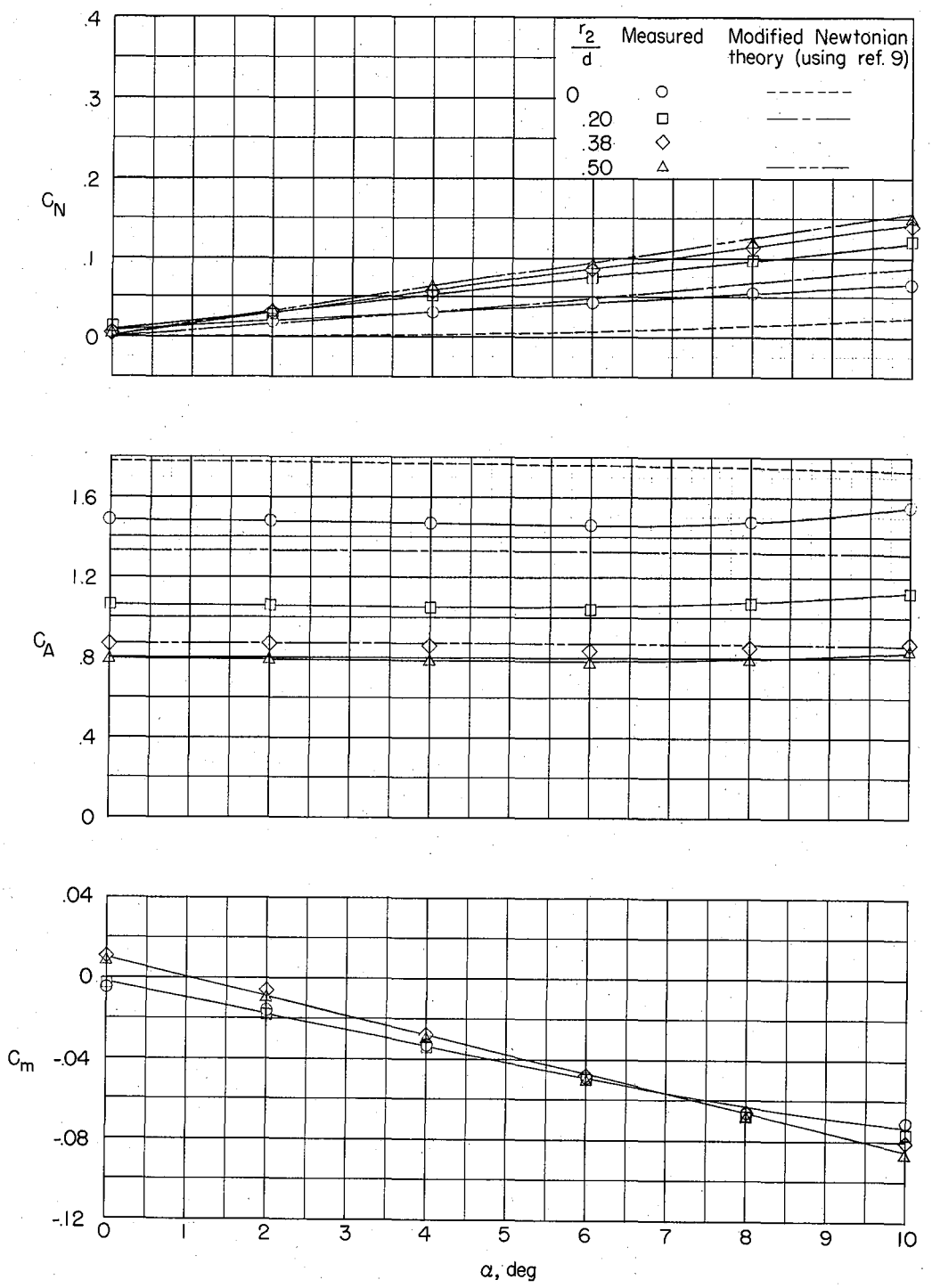

Figure 3.- Effects on C_N, C_A, and C_m of varying the corner radius of flat-faced cylinder having $l/d = 0.50$.

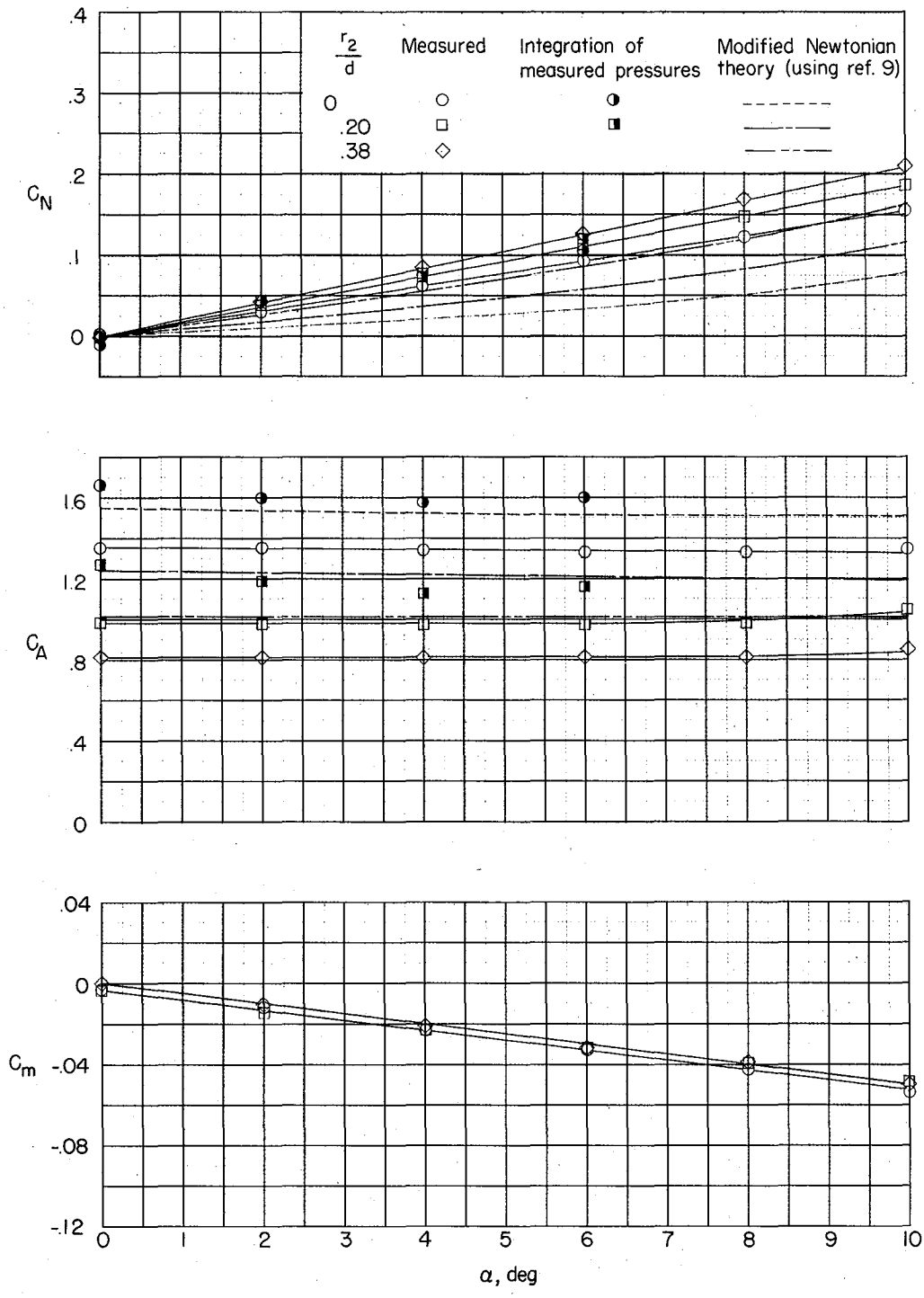

Figure 4.- Effects on C_N, C_A, and C_m of varying the corner radius of spherical-faced $(r_1/d = 1.00)$ cylinder having $l/d = 1.00$.

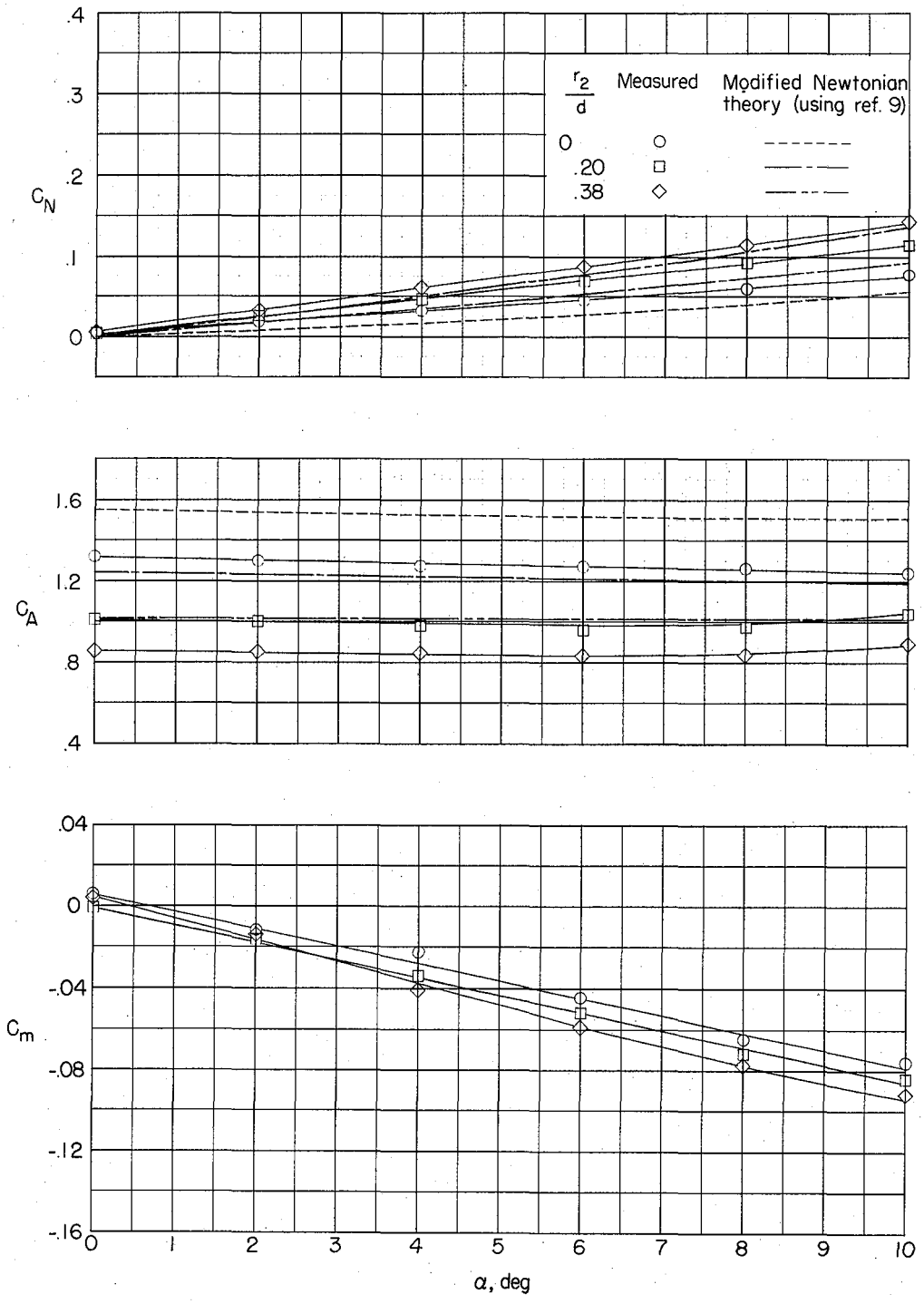

Figure 5.- Effects on C_N, C_A, and C_m of varying the corner radius of spherical-faced $(r_1/d = 1.00)$ cylinder having $l/d = 0.50$.

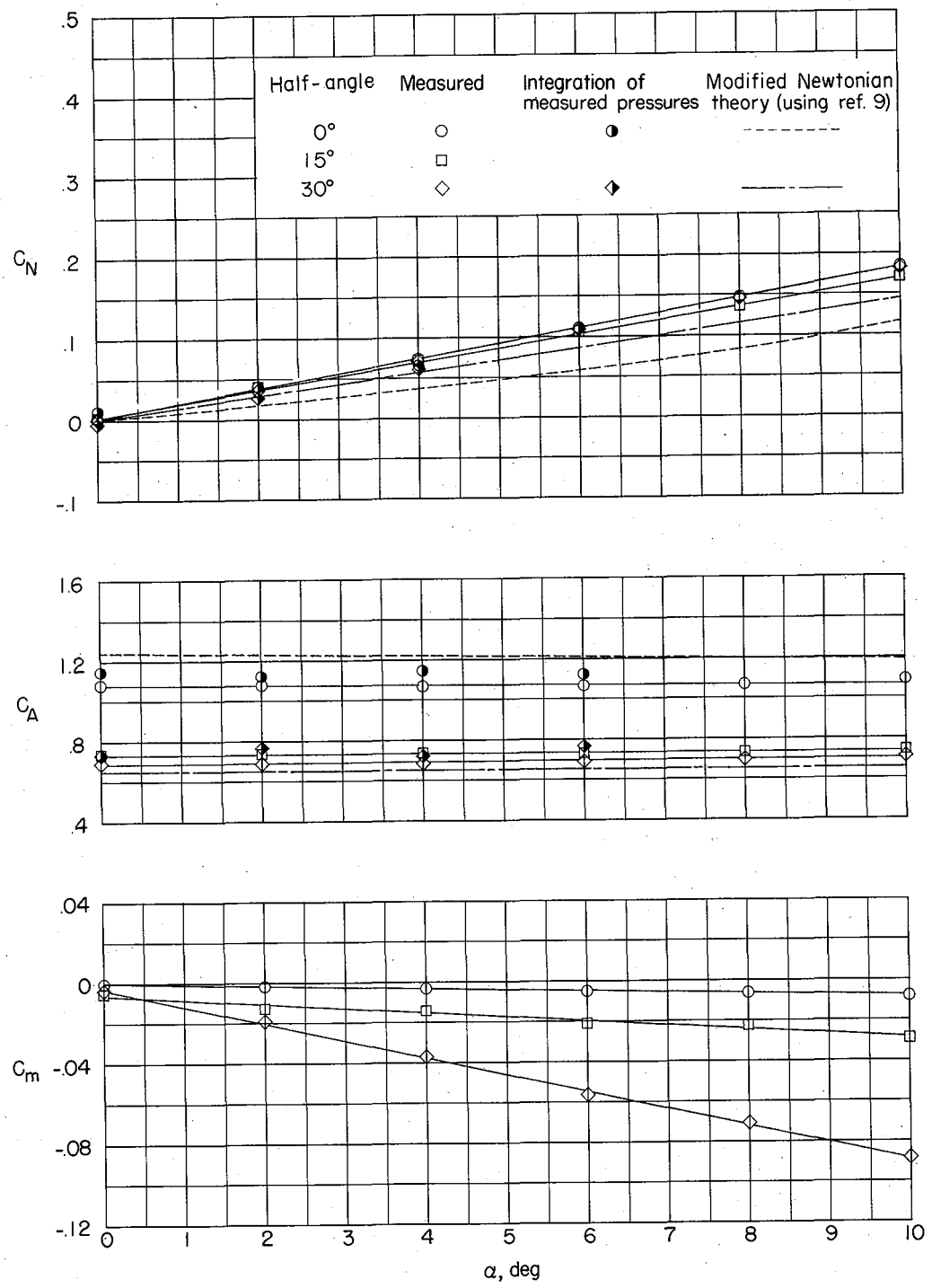

Figure 6.- Effects on C_N, C_A, and C_m of varying the half-angles of cylinder-cone frustums. For half-angle of 0°, $l/d = 1.00$.

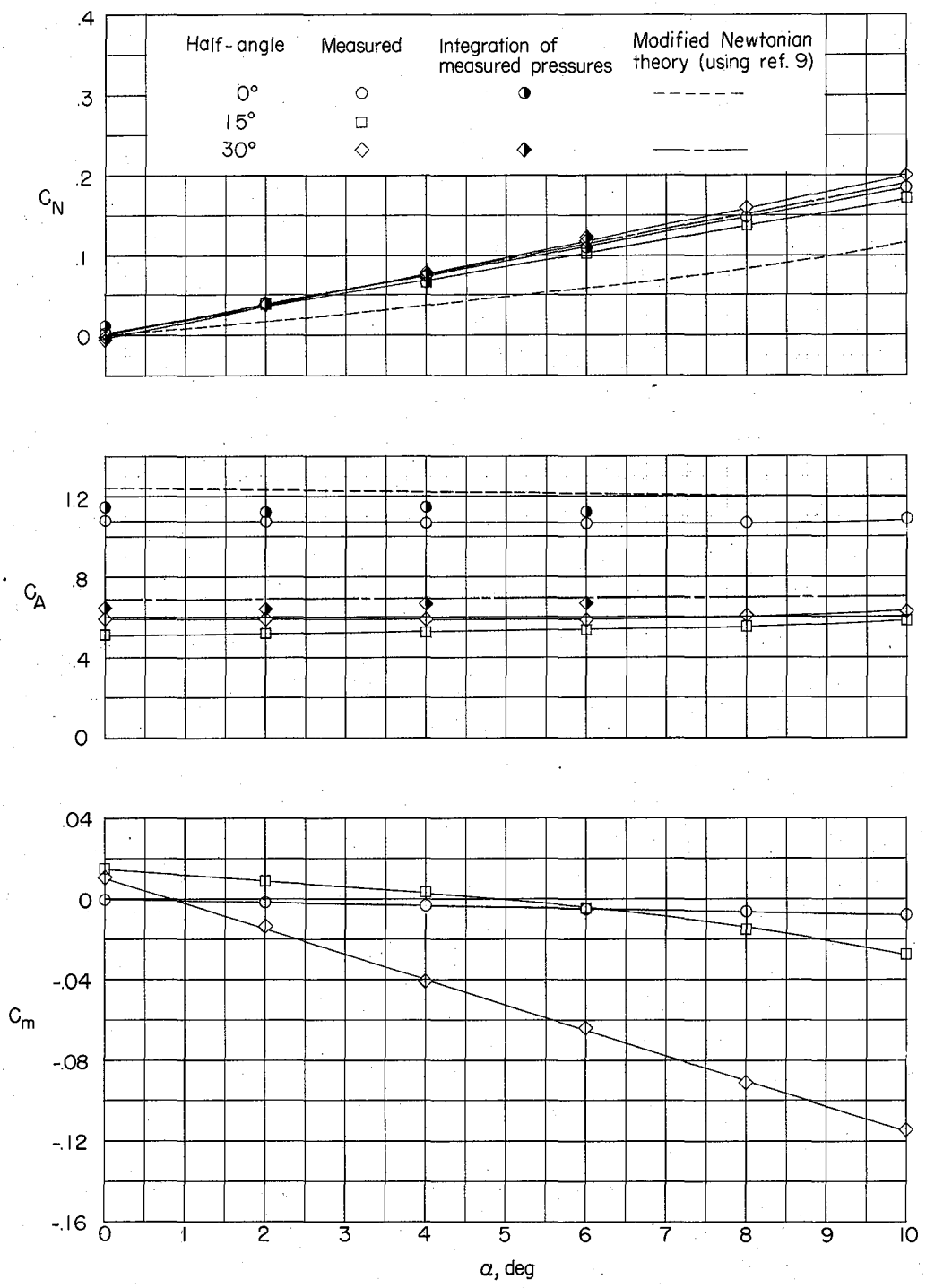

Figure 7.- Effects on C_N, C_A, and C_m of varying the half-angles of spherical-faced cone frustums. For half-angle of 0°, $l/d = 1.00$.

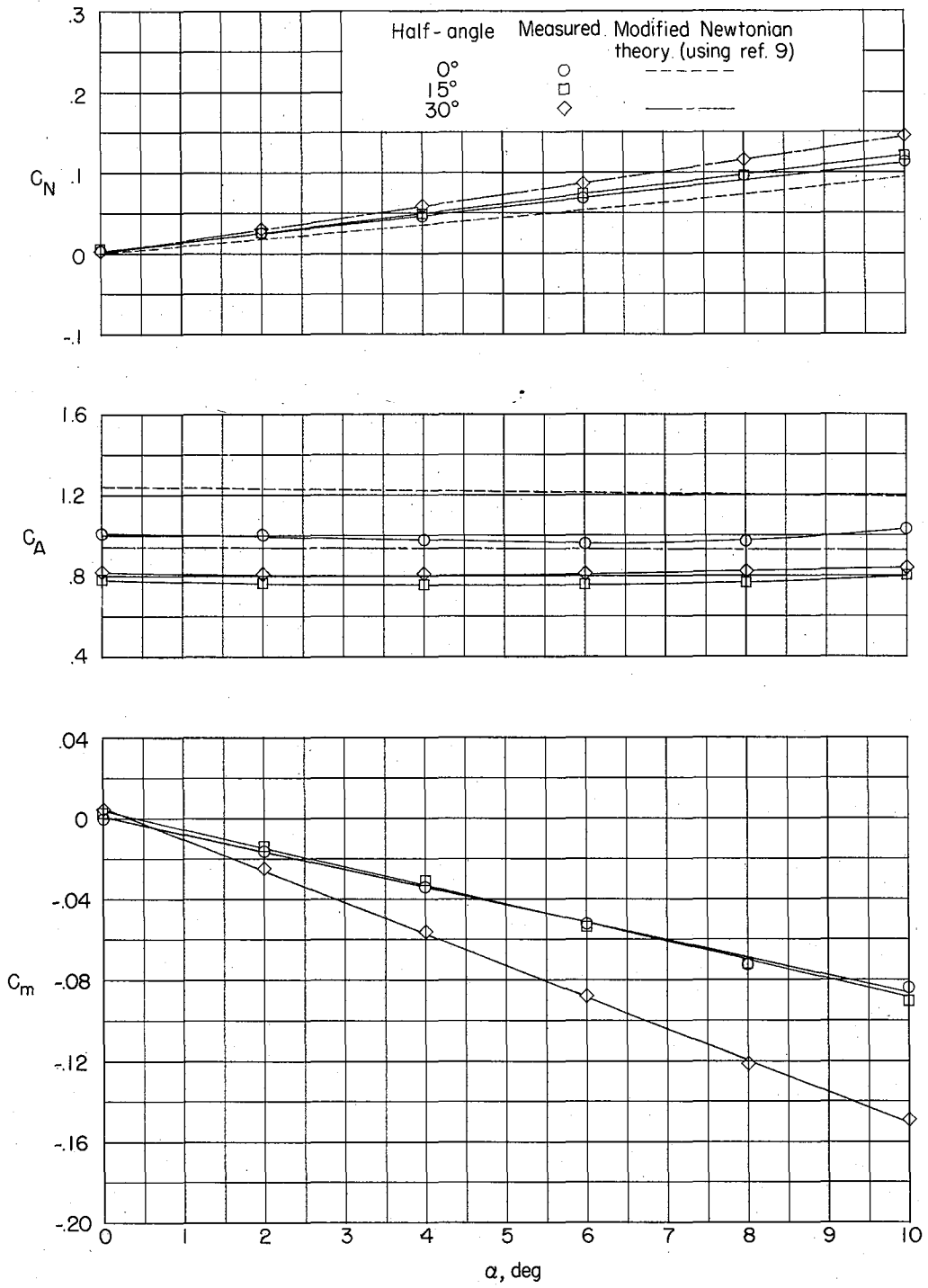

Figure 8.- Effects on C_N, C_A, and C_m of varying the half-angles of spherical-faced cone frustums. For half-angle of 0°, $l/d = 0.50$.

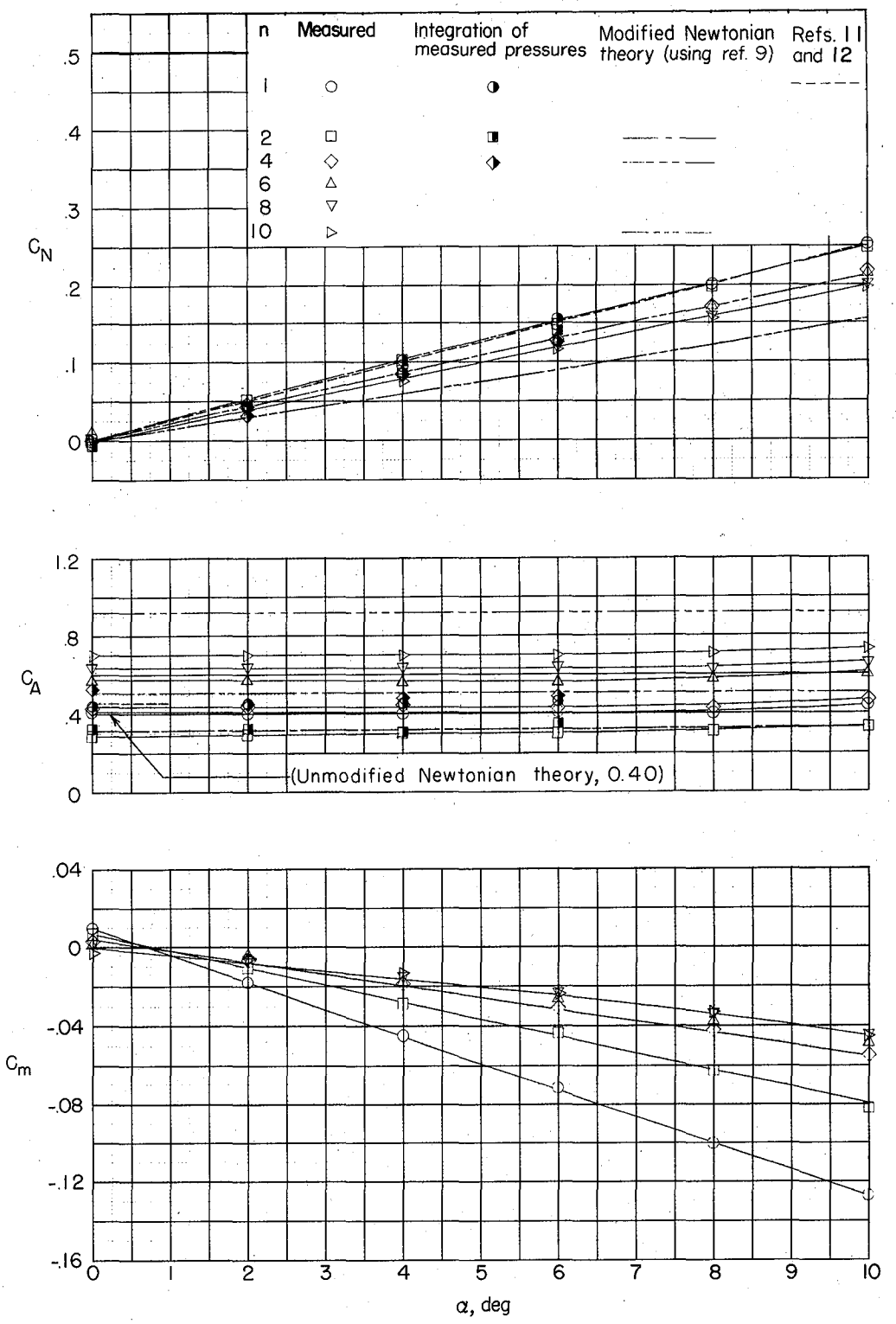

Figure 9.- Effects on C_N, C_A, and C_m of varying n for shapes defined by the equation $x = ar^n$ **having** $l/d = 1.00$.

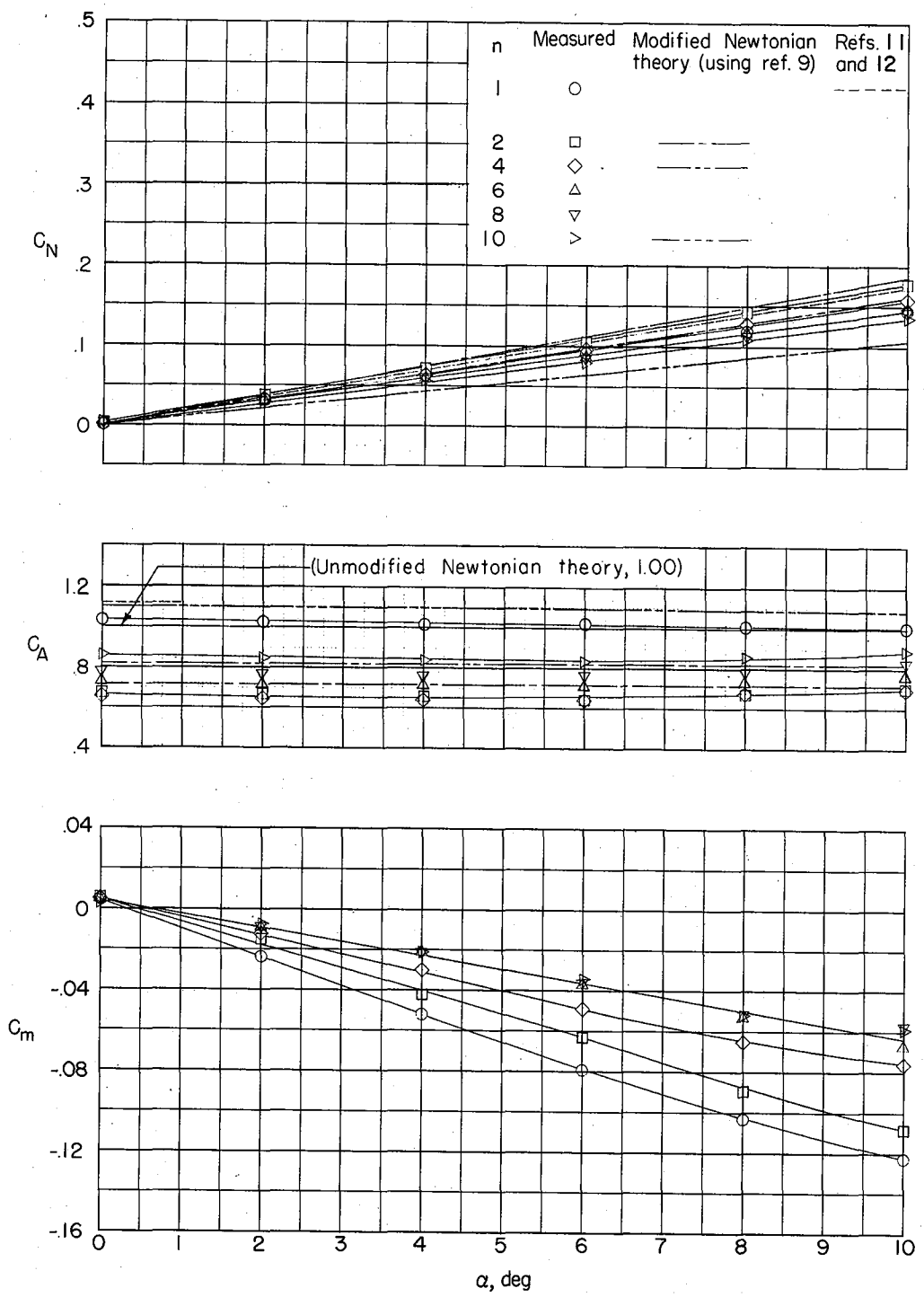

Figure 10.- Effects on C_N, C_A, and C_m of varying n for shapes defined by the equation $x = ar^n$ having $l/d = 0.50$.

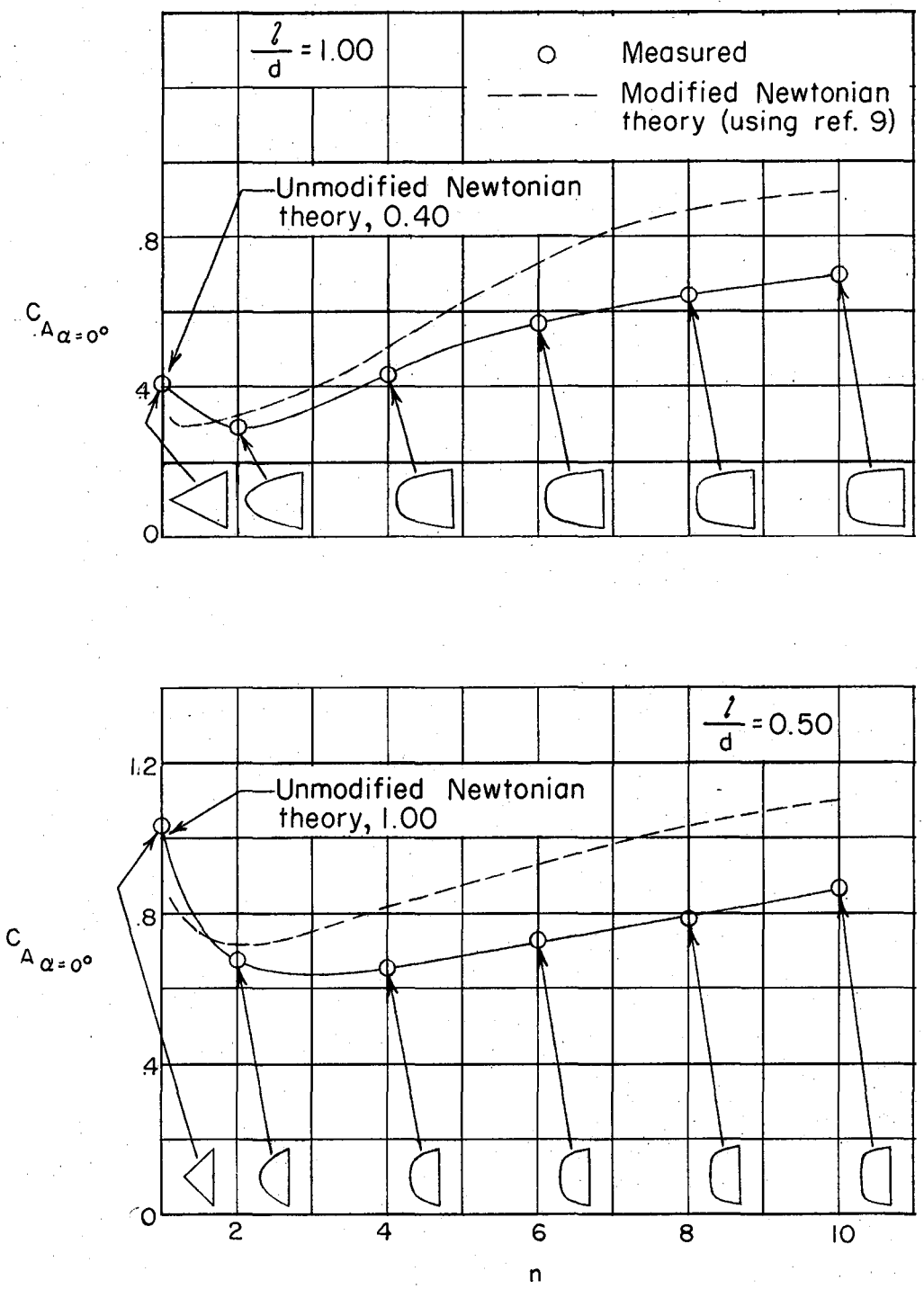

Figure 11.- Variations of $C_{A_{\alpha=0°}}$ with the exponent for exponential shapes.

UNCLASSIFIED